Halogen-bonded Cocrystal Based on Tetrathiafulvalene Derivatives①

ZHAO Long[a, c] CHEN Guan-Fan[a②]
WEN Yi-Hang[b②] XIAO Xun-Wen[c]
[a] (*School of Chemistry and Chemical Engineering, Hunan University of Science and Technology, Xiangtan* 411201, *China*)
[b] (*College of Chemistry and Life Science, Zhejiang Normal University, Jinhua* 321004, *China*)
[c] (*School of Material and Chemical Engineering, Ningbo University of Technology, Ningbo* 315211, *China*)

ABSTRACT In this paper, two cocrystals **1** and **2** with the same chemical composition [L1.L2] (L1 = bis(4′-pyridyl)-TTF, L2 = 4,4′-diiodophenyl) were synthesized by slow diffusion with different solvent systems. Cocrystals **1** and **2** were characterized by single-crystal X-ray and the purity of these two cocrystals was confirmed by PXRD data. The photocurrent responses of these two cocrystals were also tested. Only cocrystal **1** could generate photocurrent signal when exposed to light. From the crystal structure analysis, the possible reason may come from the different biphenyl conformations in L2.

Keywords: tetrathiafulvalene, crystal structure, halogen bonding, photocurrent responses;
DOI: 10.14102/j.cnki.0254-5861.2011-3150

1 INTRODUCTION

Organic cocrystals combined with two or more different molecules with non-covalent interactions, such as hydrogen bonds, halogen bonds, charge transfer (CT), and π-π interaction[1]. And the cocrystal strategy is a powerful and reliable tool to prepare new solid materials. However, to get ideal cocrystal, it is usually using strong intermolecular interaction, selecting appropriate solvent and donor (D) and acceptor (A) building blocking for the assembly to the ordered structure. Therefore, the nature of organic compound and crystal engineering play a crucial role in organic cocrystals[2]. Crystal engineering has paid much attention to the cocrystal by using the hydrogen bond, coordination bond and other types of noncovalent interaction to control the directional motifs for the synthesis of functional supramolecule. Among various non-covalent interactions, halogen bonding (XB) is one of the impotent directional tools to self-assemble organic cocrystals to from various supramolecule with special properties[3, 4]. In XB bonding, the carbonbound halogen atom (Cl, Br, I) acts as an acceptor for the lonepair electrons of a heteroatom (*i.e.*, N, O, P, S). Halogen bond-driven cocrystalli- zation could also be a tool for generating functional materials, such as catalysis, sensors, organic optoelectronic materials, and so on[5-7].

Tetrathiafulvalene (TTF) and its derivatives have been used as a type of excellent redox-active ligands to construct multifunctional materials due to their excellent reversible redox properties[8-10]. However, the solid-solid of neutral TTF-based molecule is usually governed by van der Waals force which has no direction. As a result, the polymorphs of the crystals have uncontrolled structure formation[11]. Chemists have paid much attention to introduce addition interaction sites or substituents to the TTF core, which is an efficient way for directing the supramolecular assembly and offering multifunctional molecular materials[12, 13]. The pyridyl group could not only act as a coordination group for the chelating ability to metal ions, but also be used as an acceptor unit for the halogen bond with a halogen atom (Cl, Br, I)[14]. Recently, Dai and our group have reported a new type of TTF molecule, in which the pyridine is directly linked to the TTF core, as a new ligand which is an analogue of 4,4-bipyridine[15, 16]. Moreover, novel MOFs compounds based on the ligand are reported, which show redox-active and photoelectric proper-

Received 2 February 2021; accepted 24 May 2021 (**CCDC 2060579 for 1 and 2060580 for 2**)
① This work was supported by Natural Science Foundation of Zhejiang Province (LYY20B020032) and Ningbo Science and Technology Innovation 2025(2018B10033)
② Corresponding authors. Prof. Chen Guan-Fan. E-mail: chenguanfan@126.com
Prof. Wen Yi-Hang. E-mail: wyh@zjnu.edu.cn

ties. But the cocrystals based on the ligand, especially assembled by the XB bond, are relatively rare.

We herein selected bis(4′-pyridyl)-TTF [$TTF(py)_2$][17] as the functional ligands to synthesize two novel XB bond base cocrystals. The photoelectric active electrodes of them were prepared, and their photocurrent properties were also studied.

2 EXPERIMENTAL

All reagents and solvents were obtained from commercial channels with reagent grade and used directly without further purification. And the ligand L1 was prepared according to the reported method[11]. The chemical structures of L1 and L2 are shown in Scheme 1. The PXRD data of compounds **1** and **2** were collected by Bruker D8 focus X-ray diffractometer with Cu$K\alpha$ radiation of wavelength λ = 1.5418 Å in the scanning range of 2θ from 5° to 90° at room temperature. CHI660E electrochemical workstation was used to carry out the photocurrent response experiments.

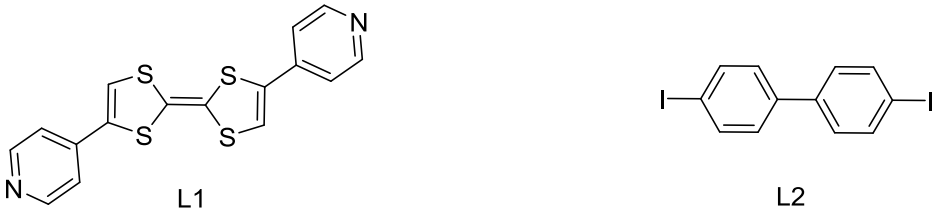

Scheme 1. Chemical structures of L1 and L2

2. 1 Synthesis

2. 1. 1 Synthesis of compound 1

The bis(4′-pyridyl)-TTF, L1 (36.0 mg, 0.1 mmol), 4,4′-diiodophenyl and L2 (42.0 mg, 0.1 mmol) were dissolved in 10 mL CH_2Cl_2 and stirred for 30 mins. Slow diffusion of n-hexane into the resulting solution at room temperature afforded deep-red crystals of XB compound **1**. Crystals were washed and filtered with hexane and dried at room temperature. 16.4 mg, yield: 21% based on L1. Anal. Calcd. (%) for $C_{14}H_9INS_2$: C, 43.98; H, 2.37; N, 3.66. Found (%): C, 43.96; H, 2.34; N, 3.67.

2. 1. 2 Synthesis of compound 2

Compound **2** was prepared by a similar method to **1** expect the slow diffusion solvent change from n-hexane to ether. Dark red crystals were obtained. Crystals were washed and filtered with ether and dried at room temperature. 19.5 mg, Yield: 25% based on L1. Anal. Calcd. (%) for $C_{24}H_{19}CdN_2O_7S_4$: C, 41.90; H, 1.31; N, 3.49. Found (%): C, 41.87; H, 1.35; N, 3.45.

2. 2 Structure determination

A suitable single crystal was selected for data collection performed on a Bruker APEX-II CCD diffractometer equipped with graphite-monochromatic Mo$K\alpha$ radiation (λ = 0.71073 Å) at room temperature. The software of CrysAlisPro Agilent Technology was used for collecting the frames of data, indexing the reflections, and determining the lattice constants, absorption correction and data reduction[18]. Using Olex2[19], the structure was solved by the ShelXT[20] structure solution program using Intrinsic Phasing and refined by full-matrix least-squares method with the SHELXL[21] on F^2. All non-hydrogen atoms were refined anisotropically. Hydrogen atoms were located using the geometric method. Compound **1** crystallizes in triclinic system, space group $P\bar{1}$ with a = 7.2592(2), b = 9.1334(3), c = 10.5281(4) Å, V = 677.40(4) Å^3, Z = 2, $C_{14}H_9INS_2$, M_r = 382.24, D_c = 1.874 g/cm^3, F(000) = 370, the final R = 0.0204 and wR = 0.0602 for 3110 observed reflections ($I > 2\sigma(I)$). Compound **2** is of monoclinic system, space group $P\bar{1}$, with a = 9.4548(6), b = 9.5677(6), c = 15.6249(10) Å, V = 1377.44(15) Å^3, Z = 4, $C_{14}H_9INS_2$, M_r = 382.24, D_c = 1.843g/cm^3, F(000) = 740, the final R = 0.0430 and wR = 0.0469 for 6361 observed reflections ($I > 2\sigma(I)$). Selected bond distances and bond angles are listed in Table 1.

2. 3 Electrode preparation and photocurrent measurement

Photocurrent response experiments were tested by CHI660C electrochemistry workstation. Cocrystals **1** and **2** were stuck evenly on ITO glass (1.0 cm × 1.0 cm, 100 Ω/mL). A 150 V Xe lamp served as light source, which is 20 cm away from the ITO electrode. ITO glass coated with samples was installed as the working electrode, Pt as the counter electrode, and saturated calomel electrode (SCE) as the reference electrode. 0.1 M Na_2SO_4 solution was used as the supporting electrolyte with the impressed voltage to be 0.8 V. The light

source keeps working continuously, and the illumination and shielding of the light source to the sample are manually controlled through a light shielding plate. The sample was measured and recorded at an interval of 20 s.

Table 1. Selected Bond Lengths (Å) and Bond Angles (°) for 1 and 2

Cocrystal **1**					
Bond	Dist.	Bond	Dist.	Bond	Dist.
I(1)–C(14)	2.103(2)	C(9)–C(14)	1.375(4)	C(10)–C(11)	1.386(3)
C(11)–C(11)#1	1.490(5)	S(1)–C(1)	1.727(3)	S(1)–C(2)	1.727(3)
C(1)–C(1)#2	1.337(5)	C(4)–C(5)	1.390(4)	C(5)–C(6)	1.376(4)
C(7)–C(8)	1.398(4)	N(1)–C(7)	1.309(5)	N(1)–C(6)	1.322(5)
Angle	(°)	Angle	(°)	Angle	(°)
C(10)–C11–C(11)#1	121.5(3)	C(12)–C(11)–C(11)#1	121.8(3)	C(9)–C(14)–I(1)	119.66(19)
C(13)–C(14)–I(1)	121.14(19)	C(2)–S(1)–C(1)	94.55(12)	C(7)–N(1)–C(6)	116.6(3)
C(1)–C(1)#2–S(1)	122.1(3)	C(1)–C(1)#2–S(2)	123.7(3)	C(4)–C(3)–S(2)	117.96(19)
C(8)–C(4)–C(3)	122.2(2)	C(8)–C(4)–C(5)	116.4(3)	C(6)–C(5)–C(4)	119.7(3)
N(1)–C(6)–C(5)	124.0(3)	N(1)–C(7)–C(8)	124.0(3)	C(4)–C(8)–C(7)	119.3(3)
Cocrystal **2**					
Bond	Dist.	Bond	Dist.	Bond	Dist.
I(1)–C(18)	2.112(4)	I(2)–C(9)	2.101(4)	S(1)–C(27)	1.741(4)
S(1)–C(26)	1.762(4)	N(1)–C(21)	1.310(8)	N(1)–C(25)	1.319(9)
N(2)–C(6)	1.301(8)	N(2)–C(7)	1.317(9)	C(1)–C(1)#3	1.357(8)
C(21)–C(22)	1.394(7)	C(22)–C(23)	1.380(7)	C(27)–C(27)#4	1.388(8)
Angle	(°)	Angle	(°)	Angle	(°)
C(27)–S(1)–C(26)	94.57(19)	C(1)–S(3)–C(2)	95.07(19)	C(21)–N(1)–C(25)	115.5(5)
C(6)–N(2)–C(7)	115.3(5)	S(3)–C(1)–S(4)	114.6(2)	C(1)#3–C(1)–S(3)	123.1(4)
C(1)#3–C(1)–S(4)	122.3(4)	C(3)–C(2)–S(3)	116.4(3)	C(4)–C(2)–S(3)	118.2(3)
N(2)–C(6)–C(5)	124.8(6)	C(10)–C(9)–I(2)	118.8(3)	C(14)–C(9)–I(2)	121.5(3)
C(13)–C(12)–C(15)	121.7(4)	C(14)–C(13)–C(12)	121.8(4)	C(17)–C(18)–I(1)	120.8(3)
C(19)–C(18)–I(1)	118.7(3)	N(1)–C(21)–C(22)	123.3(6)	C(23)–C(22)–C(21)	120.2(5)
C(22)–C(23)–C(26)	122.3(4)	C(24)–C(23)–C(22)	115.6(5)	C(27)#4–C(27)–S(1)	122.6(4)

Symmetry codes: #1: 3–*x*, –*y*, 2–*z*; #2: –*x*, 1–*y*, –*z*; #3: 2–*x*, 2–*y*, 3–*z*; #4: –1–*x*, –*y*, –1–*z*

3 RESULTS AND DISCUSSION

3. 1 Description of the crystal structures

Cocrystals **1** and **2** have been stabilized in the solid state through strong halogen bonding N–I interactions, with the N atom from the pyridine of bis(4′-pyridyl)-TTF and I from 4,4′-diiodophenyl. The N–I distances in cocrystals **1** and **2** range from 3.076 to 3.033 Å, which are shorter than the sum of van der Waals radii for nitrogen (1.55 Å) and iodine (1.98 Å)[22]. The N–I interactions are approximately linear, with the angles ranging from 174.49 to 175.20°. Selected bond lengths and bond angles for **1** and **2** are listed in Table 2.

1 was obtained as a deep-red block crystal from a CH_2Cl_2/hexane solvent system by slow diffusion method and belongs to the triclinic space group $P\bar{1}$. For **1**, half of each L1 and L2 molecule was found in the asymmetric unit (Fig. 1a). X-ray diffraction data revealed that two components of the co-crystal assemble into a 1*D* chain held together by I–N halogen bonds (I–N (Å): 3.09 Å) (Fig. 1b). These interactions lead to segregated stacking of L1 and L2. Along the *c*-axis, L1 and L2 molecules are found to from a segregated stacking mode and the interlayer distances are 3.697 Å for L1 and 3.263 Å L2, respectively. The dihedral angle of the two phenyl groups in L2 is almost 0°, implying they are coplanar (Fig. 1c).

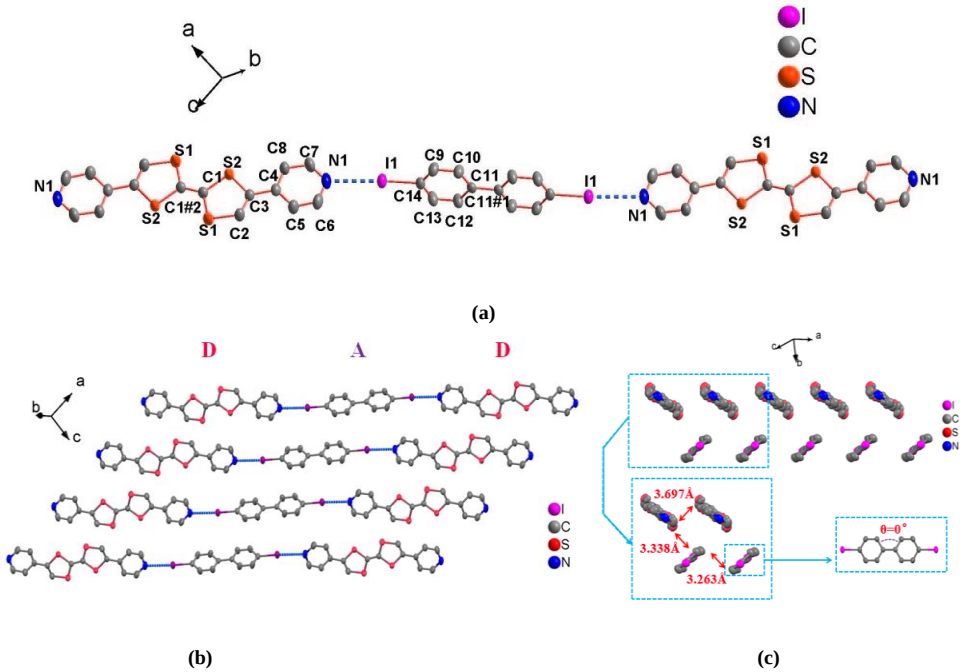

(a) **(b)** **(c)**

Fig. 1. (a) One-dimensional chain structure of 1, (b) Intermolecular stacking of 1, (c) Fragment of a supramolecular halogen-bonded chain in the structure of 1. Halogen bonds are shown as blue dotted lines

2 was obtained as a dark red block crystal from a CH_2Cl_2/ether solvent system by slow diffusion method and belongs to the triclinic space group $P\bar{1}$, For **2**, one of each bis (4′-pyridyl)-TTF and 4,4′-diiodophenyl molecules was found in the asymmetric unit. X-ray diffraction data revealed that the two components of the co-crystal assemble into a 1*D* chain held together by I–N halogen bonds (I–N (Å): 3.03 to 3.07 Å) (Fig. 2a). These interactions lead to segregated stacking of L1 and L2. Along the *c*-axis, L1 and L2 molecules are found to from a segregated stacking mode with the interlayer distances being 3.574 Å for L1 and 3.349 Å L2, respectively (Fig. 2b). The dihedral angle of the two phenyl groups in L2 being 38.95 ° means the two phenyl conformations is “non-planar”, and the segregated distances of L1 and L2 have some differences (Fig. 2c).

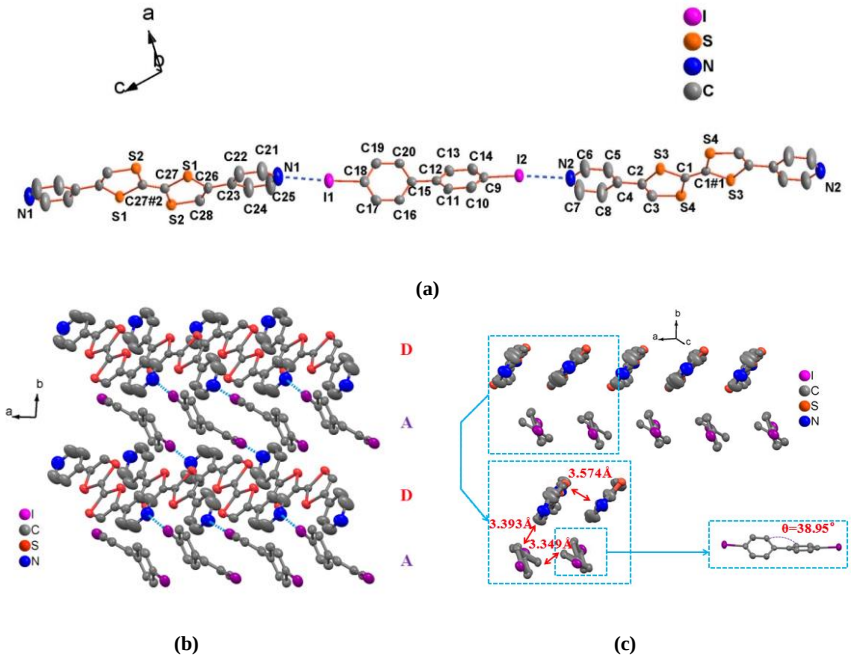

(a) **(b)** **(c)**

Fig. 2. (a) One-dimensional chain structure of 2, (b) Intermolecular stacking of 2, (c) Fragment of a supramolecular halogen-bonded chain in the structure of 2. Halogen bonds are shown as blue dotted lines

3. 2 PXRD and photocurrent response properties

3. 2. 1 PXRD analyses

In addition to elemental analysis, powder patterns for the bulk samples were compared with the calculated patterns from the crystal structures to verify the purity of the samples. The experiment data of compound **1** and **2** fit well with those simulated from the single crystal, as shown in Figs. 3a and 3b. Furthermore, the main peaks in Fig. 3 match well, which may also confirm the purity phase of these two cocrystals.

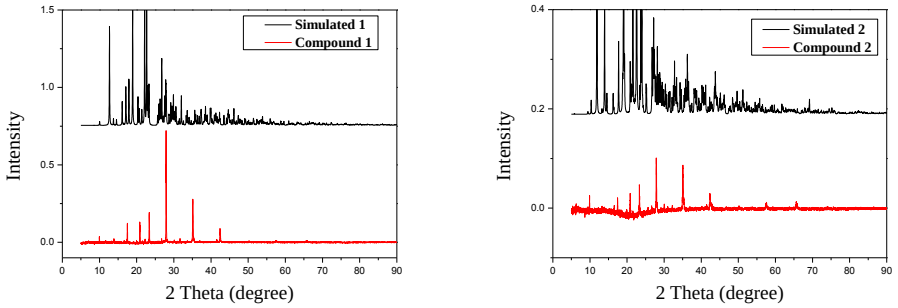

(a) **(b)**

Fig. 3. XRD patterns for the experimental and calculated results of compounds 1 and 2 (The above is for the calculated and the below for the experimental data)

3. 2. 2 Photocurrent response properties

Cyclic voltammetry experiments were carried out to test the electrochemical properties of cocrystals **1** and **2**. The precursor L1 displayed two single electron redox couples, $E^1_{1/2}$ = 0.62 V ($TTF^{\cdot}$+/TTF) and $E^2_{1/2}$ = 0.91 V (TTF^{2}+/$TTF^{\cdot}$+), which are similar to that of other TTF derivative. Compared with L1, two reversible pairs of single electron oxidation potentials could also be found, $E^1_{1/2}$ = 0.61 V ($TTF^{\cdot}$+/TTF) and $E^2_{1/2}$ = 0.92 V (TTF^{2}+/$TTF^{\cdot}$+) for **1** and $E^1_{1/2}$ = 0.61 V ($TTF^{\cdot}$+/TTF) and $E^2_{1/2}$ = 0.90 V (TTF^{2}+/$TTF^{\cdot}$+) for **2** (Fig. 4).

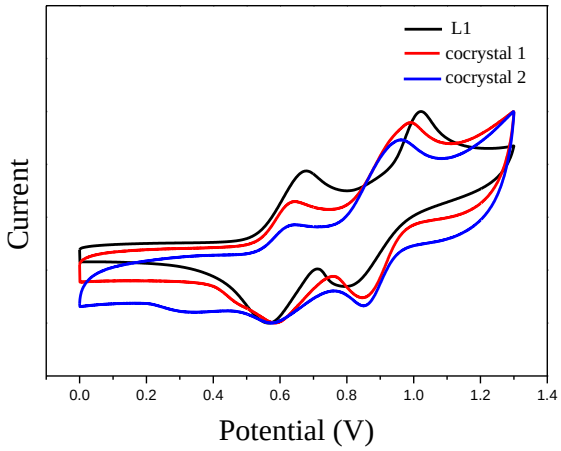

Fig. 4. Cyclic voltammograms of complexes 1, 2 and L1

In cocrystals **1** and **2**, only the two phenyl conformations in L2 are different, so the cyclic voltammetry of **1** and **2** is almost the same with that of ligand L1. These results illustrated that cocrystals **1** and **2** show redox-active properties and are easy to oxidize. Even though the donor-acceptor (D-A) compounds based on TTF derivatives usually show photoelectroactivity, there are still no TTF-based XB cocrystal with photocurrent response property to be reported. The photocurrent measurements of cocrystal **1** and **2** were performed and shown in Fig. 5.

Once irradiated with Xe light, the photocurrent of cocrystal **1** was instantly obtained at the highest value. More, the photocurrent of **1** immediately returned to its initial level when the Xe light was off. These on-off photocurrent phenomena could repeat several times, which hints that cocrystal **1** is stable enough in such conditions. However, we could not observe this phenomenon in cocrystal **2**. The results

may come from the different packing mode and the two phenyl conformations in L2 of the cocrystals. And the coplanarity of the two phenyl conformations in L2 may positivize the effectively photoinduced electron transfer process.

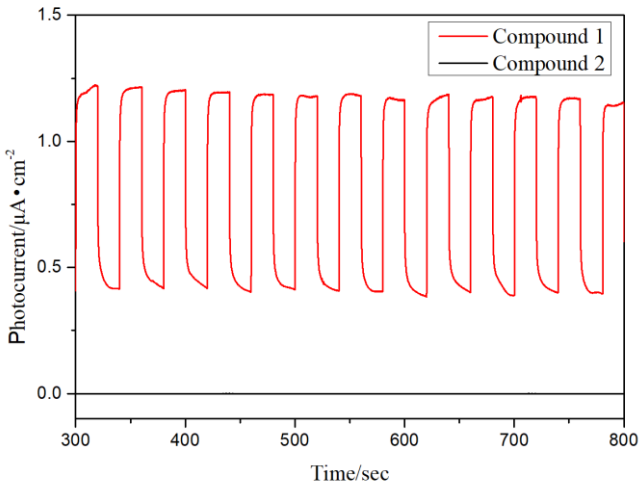

Fig. 5. Photocurrent responses of 1 and 2

4 CONCLUSION

We have successfully prepared two new cocrystals based on TTF derivatives by slow diffusion with different solvent systems. We found that the cocrystal packing modes were different due to the change of solvent system. And the results of photocurrent based on cocrystals **1** and **2** were studied, suggesting that the crystal packing greatly affects the photocurrent intensity. The coplanarity of the biphenyl conformations in L2 may be preferable for the photoelectron conversion.

REFERENCES

(1) Jimbo, T.; Tsuji, M.; Taniguchi, R.; Sada, K.; Kokado, K. Control of aggregation-induced emission from a tetraphenylethene derivative through the components in the co-crystal. *Cryst. Growth Des*. **2018**, 18, 3863−3869.

(2) Chen, S.; Zeng, X. Design of ferroelectric organic molecular crystals with ultrahigh polarization. *J. Am. Chem. Soc*. **2014**, 136, 6428−6436.

(3) Sgarbossa, P.; Bertani, R.; Di Noto, V.; Piga, M.; Giffin, G. A.; Terraneo, G.; Pilati, T.; Metrangolo, P.; Resnati, G. Interplay between structural and dielectric features of new low k hybrid organic-organometallic supramolecular ribbons. *Cryst. Growth. Des.* **2012**, 12, 297−305.

(4) Mukherjee, A.; Sanz-Matias, A.; Velpula, G.; Waghray, D.; Ivasenko, O.; Bilbao, N.; Harvey, J.; Mali, K.; De Feyter, S. Halogenated building blocks for 2*D* crystal engineering on solid surfaces: lessons from hydrogen bonding. *Chem. Sci.* **2019**, 10, 3881−3891.

(5) Cavallo, G.; Metrangolo, P.; Milani, R.; Pilati, T.; Priimagi, A.; Resnati, G.; Terraneo, G. The halogen bond. *Chem. Rev.* **2016**, 116, 2478−2601.

(6) Robertson, C. C.; Wright, J. S.; Carrington, E. J.; Perutz, R. N.; Hunter, C. A.; Brammer, L. Hydrogen bonding vs. halogen bonding: the solvent decides. *Chem. Sci*. **2017**, 8, 5392−5398.

(7) Zheng, X.; Xiao, N.; Long, Z.; Wang, L.; Ye, F.; Fang, J.; Shen, L.; Xiao, X. Hydrogen bonded-directed pure organic frameworks based on TTF-tetrabenzoic acid and bipyridine base. *Synth. Met.* **2020**, 263,116365−7.

(8) Ding, H.; Li, Y.; Hu, H.; Sun, Y.; Wang, J.; Wang, C.; Wang, C.; Zhang, G.; Wang, B.; Xu, W.; Zhang, D. A Tetrathiafulvalene-based electroactive covalent organic framework. *Chem. Eur. J*. **2014**, 20, 14614−14618.

(9) Su, J.; Yuan, S.; Wang, T.; Lollar, C. T.; Zuo, J.; Zhang, J.; Zhou, H. Zirconium metal-organic frameworks incorporating tetrathiafulvalene linkers: robust and redox-active matrices for in situ confinement of metal nanoparticles. *Chem. Sci.* **2020**, 11, 1918−1925.

(10) Canevet, D.; Sallé, M.; Zhang, G.; Zhang, D.; Zhu, D. Tetrathiafulvalene (TTF) derivatives: key building-blocks for switchable processes. *Chem. Commun.* **2009**, 2245−2269.

(11) Sun, J.; Lu, X.; Shao, J.; Li, X.; Zhang, S.; Wang, B.; Zhao, J.; Shao, Y.; Fang, R.; Wang, Z.; Yu, W.; Shao, X. Molecular and crystal structure diversity, and physical properties of tetrathiafulvalene derivatives substituted with various aryl groups through sulfur bridges. *Chem. Eur. J.* **2013**, 19, 12517−12525.

(12) Shen, W.; Xiao, X.; Ye, F.; Wang, M.; Wen, Y. Synthesis, structure and electric property of a 3*D* supramolecular Co^{II} coordination complex. *Chin. J. Struct. Chem*. **2018**, 37, 1829−1833.

(13) Narayan, T. C.; Miyakai, T.; Seki, S.; Dincă, M. High charge mobility in a tetrathiafulvalene-based microporous metal-organic framework. *J. Am. Chem. Soc*. **2012**, 134, 12932−12935.

(14) Xu, J.; Xiao, X.; Deng, K.; Zeng, Q. Transformation of self-assembly of a TTF derivative at the 1-phenyloctane/HOPG interface studied by STM-from a nanoporous network to a linear structure. *Nanoscale* **2016**, 8, 1652−1657.

(15) Wang, H.; Ge, J.; Hua, C.; Jiao, C.; Wu, Y.; Leong, C. F.; D'Alessandro, D. M.; Liu, T.; Zuo, J. Photo- and electronically switchable spin-crossover iron(II) metal-organic frameworks based on a tetrathiafulvalene ligand. *Angew. Chem. Int. Ed.* **2017**, 56, 5465−5470.

(16) Wang, R.; Kang, L.; Xiong, J.; Dou, X.; Chen, X.; Zou, J.; You, X. Structures and physical properties of oligomeric and polymeric metal complexes based on bis(pyridyl)-substituted TTF ligands and an inorganic analogue. *Dalton Trans*. **2011**, 40, 919–926.

(17) Xu, J.; Li, Y.; Wang, L.; Zhu, X.; Xiao, X.; Geng, Y.; Ke, D.; Zeng, Q. Hydrogen bonding networks controllable by the substitution position of tetrathiafulvalene on the pyridine ring. *Chin. Chem. Lett.* **2019**, 30, 767−770.

(18) *CrysAlisPro*. Rigaku Oxford Diffraction **2015**.

(19) Dolomanov, O. V.; Bourhis, L. J.; Gildea, R. J.; Howard, J. A. K.; Puschmann, H. OLEX2: a complete structure solution, refinement and analysis program. *J. Appl. Crystallogr*. **2009**, 42, 339–341.

(20) Sheldrick, G. SHELXT-integrated space-group and crystal-structure determination. *Acta Cryst*. **2015**, 71, 3–8.

(21) Sheldrick, G. M. A short history of SHELX. *Acta Cryst*. **2008**, A64, 112−122.

(22) Bondi, A. van der Waals volumes and radii. *J. Phys. Chem.* **1964**, 68, 441–451.